Preprints for the 31st International
Conference on Radar Meteorology,
6-12 August 2003, Seattle, WA

13.4

AN OBSERVATIONAL STUDY OF COLD SEASON MESOSCALE BAND FORMATION IN THE NORTHEAST UNITED STATES

by

David R. Novak[1], Jeff S. Waldstreicher[1], Lance F. Bosart[2]*, and Daniel Keyser[2]

[1]National Weather Service Eastern Region
Scientific Services Division
Bohemia, New York

[2]Department of Earth and Atmospheric Sciences
The University at Albany/SUNY
Albany, New York

1. INTRODUCTION:

A climatological and composite study of banded precipitation events in the northeast United States (US) during the cool season (October through April) is presented to illustrate how mesoscale band formation is influenced by extratropical cyclone evolution. Motivation for this task is provided by the knowledge that mesoscale band formation in extratropical cyclones is critical to improving quantitative precipitation forecasts since banded features can significantly affect the intensity, timing and subsequent accumulation of precipitation. Although several case studies in the northeast US have established the occurrence of significant mesoscale banding associated with frontogenesis and small moist symmetric stability (e.g., Sanders and Bosart 1985; Nicosia and Grumm 1999), no comprehensive studies establishing the frequency, variety, dynamical forcing, and environmental stability of significant mesoscale banding have been conducted. Until the relatively recent operational deployment of the WSR-88D national Doppler radar network, a lack of observational data on the scale of banded precipitation structures precluded such comprehensive investigations. In this study we will take advantage of the WSR-88D radar observations to identify mesoscale precipitation bands and to examine the life cycles of mesoscale precipitation systems embedded within extratropical cyclones.

2. METHODOLOGY:

Precipitation systems in the northeast US that exhibited greater than 25.4 mm (1 in) of rainfall, or 12.7 mm (0.5 in) liquid equivalent of snowfall, were identified as cases for potential study. The National Centers for Environmental Prediction (NCEP) Unified Precipitation Dataset (UPD) (http://www.cdc.noaa.gov/cdc/data.unified.html) and NOAA's Daily Weather Map Series were utilized as available to identify possible cases (gridded daily UPD fields are available at a 0.25 x 0.25 degree resolution for 24 h periods ending 1200 UTC). The study period was restricted to the cool season (Oct-Apr) from October 1996 to April 2001, a period of reasonably good WSR-88D data coverage. A total of 111 cases were identified during this period of which 88 cases had radar data as judged from archived radar mosaic imagery.

A subjective band classification scheme was then devised and applied to the 88 cases that had radar data. The scheme was devised after examining the archived radar mosaic imagery, consulting with operational forecasters and searching the refereed literature (e.g., Houze et al. 1976), and is shown in Table 1. Based upon a manual perusal ofthe 88 cases with radar coverage, three dominant bandcategories were identified: (1) single, (2) multi, and (3) narrowcold-frontal. To be included in either of these three categories the\bands had to last for at least 2 h.

TABLE 1. Band classification scheme.

Band Type	Band Description
Single	Linear structure > 250 km in length, ~ 20–100 km in width, with an intensity > 30 dBZ maintained for at least 2 h
Multi	> 3 finescale (5–20 km width) bands with periodic spacing and of the same spatial orientation, with intensities > 10 dBZ over the background reflectivity, maintained for at least 2 h
Narrow Cold-frontal	Narrow (10–50 km), long (> 300 km) band found along surface cold front or in the warm sector with an intensity > 40 dBZ maintained for at least 2 h
Transitory	Structure that meets all respective criteria in a given category, except one (usually the lifetime)
Undefined	Ambiguous due to bright banding or incomplete radar data
Nonbanded	None of the above criteria are met

A fourth category, transitory, was defined to represent banded precipitation structures that were lacking only one element of the first three categories, often that the structure failed to last the required 2 h. Two additional categories were defined: (5) undefined, and (6) nonbanded. The undefined category included ambiguous events (e.g., bright-banding was present) and/or incomplete radar data, while the nonbanded category was reserved for cases that met none of the criteria presented in Table 1 for the first three categories. For perspective purposes, we show in Fig. 1a and Fig. 1b, respectively, WSR-88D imagery for a single band taken at 0000 UTC 6 February 2001 and a nonbanded event taken at 1200 UTC 14 February 2000.

In order to identify and stratify band location with respect to mobile extratropical cyclones, a cyclone-relative composite of the single-banded events was developed. Surface cyclone positions at the analysis time deemed most representative of the observed banded precipitation structure as derived from available radar imagery were determined by using the NCEP/National Center for Atmospheric Research (NCAR) four-times daily gridded reanalysis fields available at a 2.5 x 2.5 degree resolution (Kalnay et al. 1996; Kistler et al. 2001). Next, cyclone-relative composites were calculated to identify flow regimes conducive to the development of single-banded and nonbanded structures. These cyclone-relative composites were generated from archived NCEP Eta model grids available on a 80 km resolution at the University at Albany. For this purpose initialized analysis grids available at 0000 and 1200 UTC and six-hour forecast grids available at 0600 and 1800 UTC were used. Code was developed to center the gridded fields at the surface cyclone position, and then to average the basic diagnostic fields of all events included in the composite at 17 levels (every 50 hPa from 1000 to 200 hPa) in cyclone-relative coordinates. Further data processing, diagnostic analysis and display was done using the GEMPAK software package. For example, we computed the saturation equivalent potential vorticity using the full wind to help assess the likelihood for vigorous mesoscale ascent in an environment of weak symmetric stability (e.g., Emanuel 1985) and the two-dimensional confluent frontogenesis after Miller (1948) to help assess to what extent regions of frontogenetically forced thermally direct

*Corresponding author address: Lance F. Bosart, University at Albany/SUNY, Department of Earth and Atmospheric Sciences, 1400 Washington Avenue, Albany, New York 12222 USA; email: bosart@atmos.albany.edu

mesoscale circulations overlapped areas of weak symmetric stability.

3. RESULTS:

(a) Band climatology

The 88 cases identified previously that had complete radar coverage could be associated with 153 banded events and nine undefined events in the 162 event sample (a further 13 nonbanded cases were also identified; Fig. 1b). A banded event was defined as the occurrence of a banded structure that met the criteria listed for the first five categories presented in Table 1. Some cases had more than one event and an average of almost two events per case was observed. Table 2 shows that single bands were the most common category, followed by transitory, narrow cold-frontal and multibands, respectively. Note also that individual cases frequently exhibited more than one banded event and occasionally more than one type of banded structure, as might occur when single-banded and multibanded structures were present with the multibands merging into one dominant single band of the type shown in Fig. 1a.

TABLE 2. Band climatology results.

Band Type	Single	Transitory	Narrow Cold-frontal	Multi	Undefined	**Total**
Events	48	40	36	29	9	**162**

Depicted in Fig. 2 is the cyclone-relative distribution of the 48 single-banded events given in Table 2. Each line in Fig. 2 represents the axis of a single band at the most representative analysis time. The results from Fig. 2 show that over 70% of the single bands cluster (at least in part) in the northwest quadrant of the cyclone, while the remaining single bands are more spread out ahead of the cyclone. These results suggest that the single bands in the northwest quadrant of the cyclone are likely occurring beneath the comma-head portion of the cyclone (as viewed from satellite imagery) while the single bands occurring ahead of the cyclone can probably be associated with the warm front.

(b) Composites

In order to compare and contrast single-banded and nonbanded events, cyclone-relative composites were developed for both types of events using the procedures described in section 2. We show in Fig. 3 the northwest quadrant band composite at the time closest to when the single bands were initiated (T = 0 h), with geography provided for reference. The composite 1000 hPa height and 1000-500 hPa thickness fields are shown in Fig. 3a. At this time the composite surface cyclone is situated near the Virginia Capes beneath the inflection point in the 1000-500 hPa thickness field, suggestive of a deepening cyclone. Shown in Fig. 3b are the composite 500 hPa heights and absolute vorticity along with the 300 hPa isotach field. Comparison of Figs. 3a,b shows that the composite cyclone is situated near the poleward-exit region of the 300 hPa jet streak, ahead of a negatively tilted 500 hPa trough, and upstream of the equatorward-entrance region of a confluent downstream jet. This flow configuration pattern is also favorable for cyclogenesis and bears some resemblance to the interacting jets cited by Kocin and Uccellini (1990) as common for northeast US snowstorms.

The 750-650 hPa layer-averaged two-dimensional (confluent) frontogenesis computed using the observed winds after Miller (1948) is shown shaded in Figs. 3c,d, along with the 700 hPa heights and layer-averaged 750-650 hPa resultant deformation in Fig. 3c and the 750-650 hPa layer-averaged temperature advection (only warm-air advection is contoured) in Fig. 3d. Note that the large-scale layer-averaged 750-650 hPa resultant deformation region encompasses the region of layer-averaged 750-650 hPa two-dimensional frontogenesis poleward and to the northwest of the composite cyclone. This location is coincident with the mean single-band position across Pennsylvania (Fig. 3d). The colocation of the mean single-band position with the axis of mean 750-650 hPa frontogenesis is suggestive that mesoscale frontogenetically forced thermally direct circulations in conjunction with warm-air advection in a near symmetrically neutral environment (not shown) are contributing favorably to mesoscale single-band formation. These findings are consistent with the results of several past studies (e.g., Emanuel 1985; Sanders and Bosart 1985; Nicosia and Grumm 1999) that have shown strong frontogenesis in the presence of vigorous ascent in an atmosphere of weak symmetric stability supports mesoscale band formation.

Next, we show in Fig. 4 the identical plot to Fig. 3 except for the nonbanded composite. The nonbanded composite cyclone is much weaker and is embedded in a much weaker 1000-500 hPa thickness trough (Fig. 4a). Absent is the deep upstream trough and jet seen in Fig. 3b in favor of a downstream confluent jet-entrance region (Fig. 4b). Although significant precipitation was associated with cases included in this composite, the absence of a closed 700 hPa circulation precluded significant deformation and frontogenesis from occurring and wrapping around to the northwest quadrant of the composite 1000 hPa cyclone (Figs. 4c,d), limiting band development. Likewise, although midlevel confluence ahead of the surface cyclone contributes to frontogenesis (as does warm-air advection; Fig. 4d), it is weaker in the lower levels than in the single-banded northwest composite (not shown).

Finally, we show cross sections of two-dimensional frontogenesis, saturated equivalent potential temperature, θ_{es}, saturated equivalent potential vorticity computed using the full wind, relative humidity and vertical velocity for the northwest single-banded (nonbanded) composite in Figs. 5a,b (Figs. 5c,d). Although frontogenetical forcing is readily evident in both cross sections, with a sloping frontogenesis maximum found along the equatorward flank of each frontal zone (Figs. 5a,c), the single-banded northwest composite cross section exhibits a stronger, narrower and deeper updraft in conjunction with a well-defined axis of higher relative humidity than the nonbanded composite cross section (Figs. 5b,d). Likewise, the θ_{es} contours appear to be somewhat more upright near the warm boundary of the frontogenesis region in the single-banded northwest composite cross section (Fig. 5a), consistent with more vigorous ascent in a zone of higher relative humidity in the same region (Fig. 5b).

4. DISCUSSION:

We summarize our findings by showing a conceptual model of single-banded vs. nonbanded cyclones in planar (Fig. 6) and cross-section (Fig. 7) formats. These conceptual models were constructed from the composite results shown in Figs. 4,5 as well as from the case study findings (not shown). In the single-banded northwest conceptual model (Fig. 6a) an area of midlevel frontogenesis and resultant deformation, situated between lower-latitude upstream and higher-latitude downstream upper-level jets, runs from near the poleward side of a midlevel cutoff cyclone eastward toward the downstream ridge axis. In the nonbanded composite the axis of midlevel frontogenesis and resultant deformation is shifted eastward ahead of the surface cyclone, poleward of the surface warm front and close to the equatorward-entrance region of the downstream upper-level jet (Fig. 6b). Schematic cross sections of frontogenesis, θ_{es} and ascent through the single-banded northwest and nonbanded composites are shown

in Figs. 7a,b, respectively. More vigorous ascent, a stronger and deeper axis of frontogenesis, and more upright θ_{es} surfaces are indicated in the northwest single-banded composite. The composite results shown in Figs. 4,5, and in schematic form in Figs. 6,7, together suggest that single bands that form under the comma head region to the northwest of the center of a surface extratropical cyclone occur in conjunction with a deep layer of frontogenesis that tends to be more vertically aligned than in the nonbanded composite. The associated more upright θ_{es} surfaces suggest that single-band formation may be favored in frontogenetically forced regions characterized by small positive symmetric neutrality and vigorous ascent in accord with the expectation of narrower, more upright, and more intense "circulation ellipses" from the well-known Sawyer-Eliassen equation.

5. ACKNOWLEDGEMENT:

Elizabeth Page and Dolores Kiessling from COMET were instrumental in providing the necessary data to undertake this study. Celeste Iovinella provided critical support in all aspects of manuscript preparation. The research was supported by NOAA Grant #NA07WA0458, awarded to the University at Albany/SUNY as part of the CSTAR program. Additional information concerning the University at Albany CSTAR project may be found at the following Web site: http://cstar.cestm.albany.edu/

6. REFERENCES:

Emanuel, K. A., 1985: Frontal circulations in the presence of small moist symmetric stability. *J. Atmos. Sci.*, **42**, 1062–1072.

Houze, R. A., J. D. Locatelli, and P. V. Hobbs, 1976: Dynamics and cloud microphysics of the rainbands in an occluded frontal system. *J. Atmos. Sci.*, **33**, 1921–1936.

Kalnay, E., M. Kanamitsu, R. Kistler, W. Collins, D. Deaven, L. Gandin, M. Iredell, S. Saha, G. White, J. Woollen, Y. Zhu, A. Leetmaa, B. Reynolds, M. Chelliah, W. Ebisuzaki, W. Higgins, J. Janowiak, K. C. Mo, C. Ropelewski, J. Wang, R. Jenne, and D. Joseph, 1996: The NCEP/NCAR 40 year reanalysis project. *Bull. Amer. Meteor. Soc.*, **77**, 437–471.

Kistler, R., E. Kalnay, W. Collins, S. Saha, G. White, J. Woollen, M. Chelliah, W. Ebisuzaki, M. Kanamitsu, V. Kousky, H. Van den Dool, R. Jenne, and M. Fiorino, 2001: The NCEP-NCAR 50-year reanalysis: Monthly means CD-ROM and documentation. *Bull. Amer. Meteor. Soc.*, **82**, 247–268.

Kocin, P. J., and L. W. Uccellini, 1990: Snowstorms along the northeastern coast of the United States, 1955-1985. American Meteorological Society, Meteor. Monogr. 22, No. 44, 280 pp.

Miller, J. E., 1948: On the concept of frontogenesis. *J. Meteor.*, **5**, 169–171.

Nicosia, D. J., and R. H. Grumm, 1999: Mesoscale band formation in three major Northeastern United States snowstorms. *Wea. and Forecasting*, **14**, 346–368.

Sanders, F., and L. F. Bosart, 1985: Mesoscale structure in the megalopolitan snowstorm of 11-12 February 1983. Part I: Frontogenetical forcing and symmetric instability. *J. Atmos. Sci.*, **42**, 1050–1061.

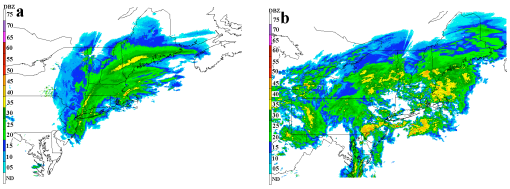

Fig. 1. WSR-88D radar mosaic of a (a) single banded and a (b) nonbanded case valid at (a) 0000 UTC 6 February 2001 and (b) 1200 UTC 14 February 2000 (color scale along left side of each image, every 5 dBZ).

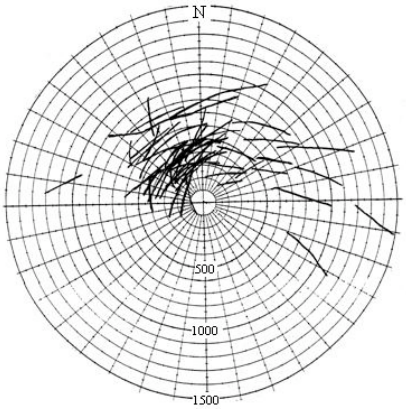

Fig. 2. Distribution of single-banded events relative to surface cyclone position (origin). Each black line represents the axis of a single band at the most representative analysis time. Geographic-relative north is denoted by the "N" at the top of the figure. The radial distance scale is in kilometers.

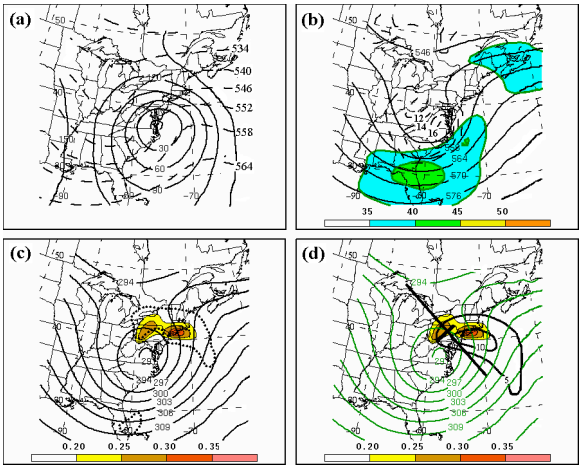

Fig. 3. Northwest composite at band initiation (time T = 0 h). (a) 1000 hPa heights (solid) every 30 m and 1000-500 hPa thickness (dashed) every 6 dam. (b) 500 hPa heights (solid) every 6 dam, absolute vorticity (dashed) every 2 x 10^{-5} s^{-1} starting at 12 x 10^{-5} s^{-1}, and 300 hPa isotachs (shaded) beginning at 35 m s^{-1}. (c) 700 hPa heights (solid) every 3 dam, 750-650 hPa layer-averaged resultant deformation (dotted) every 3 x 10^{-5} s^{-1}, and 750-650 hPa layer-averaged frontogenesis (shaded) in °C (100 km)$^{-1}$ (3 h)$^{-1}$. (d) 700 hPa heights (solid green) every 3 dam, 750-650 hPa frontogenesis (as in c), and 750-650 hPa layer-averaged temperature advection (solid black) contoured for positive values every 5 °C (day)$^{-1}$ starting at 5°C (day)$^{-1}$. Cross section orientation and mean band position for Figs. 5a,b is shown in (d).

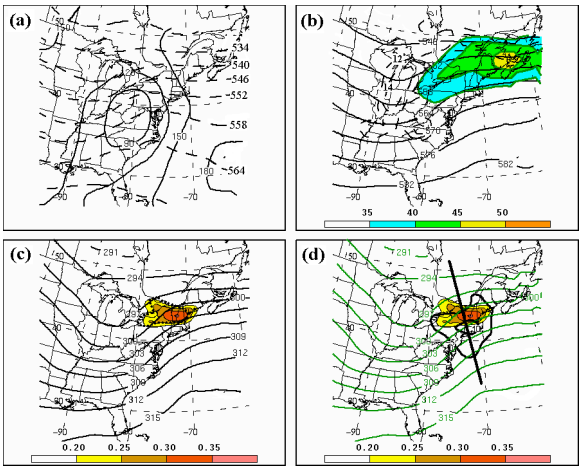

Fig. 4. As in Fig. 3 except for the nonbanded composite at T = 0 h. Cross section orientation in Figs. 5c,d is shown in (d).

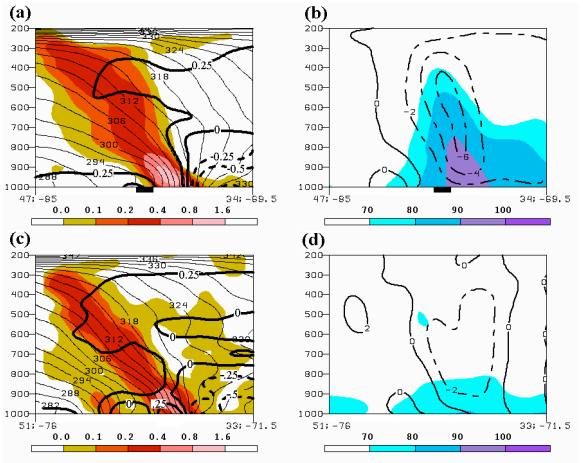

Fig. 5. (a) Cross section through the composite band position (black bar along x-axis) in the northwest single-banded composite at band initiation (time T = 0 h) showing frontogenesis (shaded for positive values according to the color scale in units of °C $(100\ km)^{-1}\ (3\ h)^{-1}$. Saturation equivalent potential temperature (thin solid) every 3 K, saturation equivalent potential vorticity computed using the full wind (heavy solid) every 0.25 PVU (1 PVU = 10^{-6} $m^2\ K\ kg^{-1}\ s^{-1}$) contoured at and below 0.25 PVU. Cross section orientation in (a) and (b) is given in Fig. 3d. (b) Relative humidity beginning at 70%, shaded according to the color scale, and vertical motion contoured every 2 x 10^{-3} hPa s^{-1} with dashed (solid) contours denoting ascent (descent); zero contour is drawn solid. (c) as in (a) except for the nonbanded composite at time T = 0 h. (d) as in (b) except for the nonbanded composite. Cross section orientation in (c) and (d) is given in Fig. 4d.

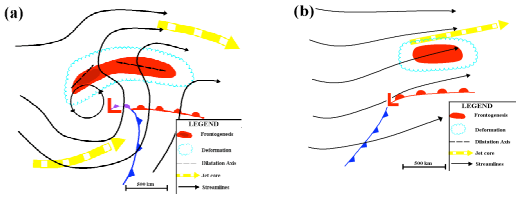

Fig. 6. Conceptual model of a (a) single-banded system and a (b) nonbanded system highlighting the key parameters. Features shown include midlevel frontogenesis (red shading), midlevel deformation zone (encompassed by scalloped line) and associated primary dilatation axes (dashed line), midlevel streamlines (black lines), and upper-level jet cores (wide dashed arrows).

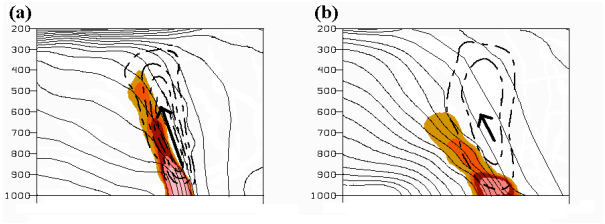

Fig. 7. Schematic cross sections through a (a) typical single-banded environment and (b) a typical nonbanded environment. Fields shown are frontogenesis (red shading), saturated equivalent potential temperature (thin solid), and ascent (dashed) with length of arrow proportional to the magnitude of ascent and orientation representative of air parcel trajectory. Cross-section length is approximately 1000 km.